JOURNAL OF APPLIED ELECTROCHEMISTRY **27** (1997) 846–856

Analysis of capacity–rate data for lithium batteries using simplified models of the discharge process

M. DOYLE*, J. NEWMAN

Energy and Environment Division, Lawrence Berkeley Laboratory and Department of Chemical Engineering, University of California Berkeley, California 94720-1462

Received 1 May 1995; revised 20 January 1997

Simplified models based on porous electrode theory are used to describe the discharge of rechargeable lithium batteries and derive analytic expressions for the specific capacity against discharge rate in terms of the relevant system parameters. The resulting theoretical expressions are useful for design and optimization purposes and can also be used as a tool for the identification of system limitations from experimental data. Three major cases are considered that are expected to hold for different classes of systems being developed in the lithium battery industry. The first example is a cell with solution phase diffusion limitations for the two extreme cases of a uniform and a completely nonuniform reaction rate distribution in the porous electrode. Next, a discharge dominated by solid phase diffusion limitations inside the insertion electrode particles is analysed. Last, we consider an ohmically-limited cell with no concentration gradients and having an insertion reaction whose open-circuit potential depends linearly on state of charge. The results are applied to a cell of the form Li|solid polymer electrolyte|$Li_yMn_2O_4$ in order to illustrate their utility.

List of symbols

a	specific interfacial area (cm^{-1})
c	concentration of electrolyte in the solution phase ($mol\,dm^{-3}$)
c_0	initial concentration in solution ($mol\,dm^{-3}$)
c_1	concentration of electrolyte in front of reaction zone ($mol\,dm^{-3}$)
c_s	concentration of lithium in the solid phase ($mol\,dm^{-3}$)
c_t	maximum concentration in solid ($mol\,dm^{-3}$)
C	specific capacity ($C\,g^{-1}$)
D	diffusion coefficient of electrolyte in the solution ($cm^2\,s^{-1}$)
D_s	diffusion coefficient of lithium in the solid electrode particles, ($cm^2\,s^{-1}$)
F	Faraday's constant ($96\,487\,C\,mol^{-1}$)
I	superficial current density ($mA\,cm^{-2}$)
j_n	pore wall flux of lithium ions ($mol\,cm^{-2}\,s^{-1}$)
J	dimensionless pore wall flux defined in Equation 8
k	slope of open-circuit potential function
L	cell component thickness (m)
M	mass per unit area of cell ($g\,cm^{-2}$)
n	parameter representative of electrode particle geometry
q	capacity density of composite positive electrode ($C\,cm^{-3}$)
r	dimensionless geometric ratio defined in Equation 8
R	universal gas constant ($8.3143\,J\,mol^{-1}\,K^{-1}$)
R_s	radius of positive electrode material (μm)
s	Laplace space variable (s^{-1})
t	time (s)
t_d	discharge time (s)
t_i^0	transference number of species i
T	temperature (K)
U	open-circuit potential (V)
V	cell potential (V)
V_c	cutoff potential (V)
x	distance from the separator/positive electrode boundary (m)
x_r	position of the reaction-zone boundary (m)
y	dimensionless distance defined in Equation 8

Greek letters

ε	porosity of electrode
Θ	dimensionless concentration defined in Equation 8
κ	ionic conductivity of electrolyte ($S\,cm^{-1}$)
ρ	density ($g\,cm^{-3}$)
τ	dimensionless time or depletion time
Φ	electrical potential (V)

Subscripts

+	positive electrode
0	initial condition
s	separator

Superscripts

0	with respect to the solvent
θ	standard cell potential

* Present address: DuPont Central Research and Development, Experimental Station, Wilmington, DE 19880-0304.

0021-891X

1. Introduction

A subject of much practical interest is the utility of capacity against rate (C/I) and energy against power (E/P) expressions for both primary [1, 2] and secondary [2–4] batteries. These correlations are useful as both a design tool and a method for prediction of battery performance under different operating conditions. It might also be possible under some conditions to identify the limiting mechanisms in a battery based on the shape of the C/I or E/P data. Correlations of these types are usually obtained from the analysis of experimental data and functional fits are developed based on empirically defined parameters with little theoretical meaning.

Capacity–rate and energy–power relationships for batteries can also be developed by using a mathematical model of a single cell to describe the current–potential behaviour. Quantities of interest, such as the capacity, energy and power, are all derived quantities from the I/V behaviour of the cell. Under certain simplified conditions, these models reduce to limiting forms allowing correlations for C/I and/or E/P data to be developed. In this way, the parameters appearing in the correlations can be related to fundamental physical properties and system specifications. Also, having started with the general mathematical description, it is possible to develop criteria for deciding when these limiting cases are applicable.

Rechargeable lithium and lithium ion cells have become commercially viable and are under consideration for electric vehicle applications. Mathematical modelling efforts have been focused on optimization of the cell design and system parameters and the thermal control of the battery module. General models have been developed to simulate the behaviour of these systems during charge, discharge and relaxation [5–7]. However, due primarily to their generality, these models are complicated, and often for particular systems a simplified treatment is possible that captures the essential features of the discharge behaviour.

In previous work, we have analysed both experimental and theoretical I/V data for a variety of lithium-based systems, including lithium metal–polymer electrolyte cells using poly(ethylene oxide) and lithium trifluoromethanesulfonate ($PEO_nLiCF_3SO_3$) or single ion conducting polymer electrolytes [5, 8], liquid lithium ion cells like the Sony cell $LiC_6|LiPF_6$, propylene carbonate, diethyl carbonate$|LiCoO_2$ [7] and gelled-electrolyte systems such as the Bellcore cell $LiC_6|LiPF_6$, ethylene carbonate, dimethyl carbonate, poly(vinylidene fluoride-hexafluoropropylene)$|LiMn_2O_4$ [6, 9]. In many cases, the E/P data follow simple models as discussed earlier. For example, the lithium–polymer cell with a single ion conducting polymer electrolyte follows the ohmically dominated battery model developed previously [10, 11]. In other cases, such as that of the Bellcore system, although the discharge behaviour of the cell is dictated by a complex interplay of ohmic and diffusion phenomena, the C/I and E/P data take more simple forms.

2. Classification of analytic solutions

We consider some limiting cases that are applicable to specific systems. These cases can be separated into two categories based on whether solution-phase concentration variations exist. The salt concentration is uniform, for example, with a system having a unity transference number [8] for the lithium ion or at very short times, much less than the diffusion time. If this is the case, the governing equations are much simpler, and several possibilities exist for the examination of approximate analytic solutions [12]. When concentration gradients can not be neglected, the situation is much more complex due to the coupled nature of the governing equations. For this reason very few analytic solutions can be found in the literature that include concentration variations in the solution phase [12, 13]; this problem is generally relegated to numerical methods.

First, we examine the latter case in which the discharge is dominated by solution-phase diffusion limitations. We neglect kinetic and solid-phase diffusion limitations and assume that the transport properties are independent of salt concentration (D and t_+^0 only, κ does not appear in the analysis). The neglect of kinetic resistances is a good assumption for the insertion electrodes often used with lithium rechargeable batteries. In addition, we focus on a system having a single insertion electrode. The generalization of the results to a lithium ion cell which employs two different insertion electrodes should be straightforward. We treat the extreme case of a completely uniform current distribution in the porous electrode. This analysis is contrasted with the Stein [14] model, which considers the transient depletion of the active species from solution at the front face of the porous electrode due to a high rate discharge: the assumption of a completely nonuniform current distribution. We also explore an intermediate approximate solution making use of a reaction zone assumption.

Next, we treat cases in which the solution-phase concentration is uniform over the time of discharge of the battery. A cell dominated by solid state diffusion limitations inside the insertion-electrode particles is treated. Diffusion coefficients for the lithium ion in insertion electrode materials are often low enough to bring about this situation. Concentration gradients in the solution phase are neglected, and a reversible charge transfer process is assumed. In addition, we assume the reaction distribution in the porous electrode is uniform. This assumption is necessary to decouple the governing equations and allow an analytic solution to be developed.

The last system discussed is an ohmically dominated cell. We assume that kinetic and solution and solid-phase diffusion limitations do not exist. With these assumptions, the system becomes similar to an

ohmically dominated porous electrode model covered previously [10, 11]. The reaction moves through the electrode as a front which consumes all of the available active material at a point before moving on. The effect of an open circuit potential that depends on the state of charge of the electrode, as in insertion compounds, is included in the treatment [15]. A similar problem has been considered by Atlung *et al.* [16, 17].

The primary goal for all the above cases is to obtain expressions for the specific capacity as a function of the discharge rate. From this information, practical design issues such as optimal electrode thicknesses and porosities can be approached.

3. Theoretical development

For all cases, the macroscopic transport through the cell sandwich is treated as one-dimensional (Fig. 1). The development is based on porous electrode theory [18], where the electrode is treated as two superimposed continua without regard for the actual geometric detail of the pore structure. The separator consists of either an inert polymer material or a nonaqueous liquid that acts as the solvent for a lithium salt. The negative electrode is a lithium foil, and the positive electrode is a porous electrode consisting of solid insertion material particles, inert conducting filler, and the solution phase. The porous electrode is assumed to have a very large electronic conductivity ($\sigma \gg \kappa$) and a large exchange current density for the insertion process. These conditions hold for typical lithium insertion electrodes under a 3 h discharge [6].

3.1. *Case I: Solution-phase diffusion limitations*

When concentration variations cannot be neglected the possibility for finding relevant analytic expressions for the specific energy is greatly diminished. However, as previous simulation results have demonstrated the importance of solution-phase diffusion limitations in the discharge of these systems [5, 6], it is useful to explore some simplified cases. The differential and algebraic equations that describe the concentration, potential and current density in the solution phase of the porous electrode are in general nonlinear and coupled [5]. To find an analytical solution we must first decouple these equations by assuming a form for the reaction rate distribution through the porous electrode. Once j_n is specified the current density and concentration profiles may be determined using the boundary and initial conditions and the potential gradient is determined from these. Figure 1 shows the coordinate axis and cell dimensions.

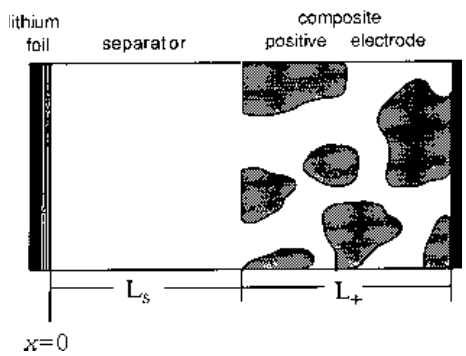

Fig. 1. Lithium/polymer cell sandwich, consisting of lithium foil negative electrode, solid polymer electrolyte, and composite positive electrode.

A material balance on the salt in the solution phase of the porous electrode gives

$$\varepsilon \frac{\partial c}{\partial t} = \varepsilon D_{\text{eff}} \frac{\partial^2 c}{\partial x^2} + a j_n (1 - t_+^0) \tag{1}$$

where the diffusivity is an effective value accounting for the actual path length of the species using the Bruggeman expression [19]

$$D_{\text{eff}} = \varepsilon^{1/2} D \tag{2}$$

There are two regions in the cell: (i) in the solution phase ($c = c_2$, $L_s \le x \le L_s + L_+$); of the porous electrode the above equations apply as written (ii) in the separator region ($c = c_1, 0 \le x < L_s$), $j_n = 0$ and $\varepsilon = 1$. For a galvanostatic discharge the boundary and initial conditions are

$$\frac{\partial c_1}{\partial x} = -\frac{I(1 - t_+^0)}{FD} \quad \text{at } x = 0 \tag{3}$$

$$\frac{\partial c_2}{\partial x} = 0 \quad \text{at } x = L_s + L_+ \tag{4}$$

$$c_1 = c_2 = c_0 \quad \text{at } t = 0 \tag{5}$$

Continuity of the concentration and flux across the separator/porous electrode internal boundary ($x = L_s$) lead to

$$c_1 = c_2 \quad \text{at } x = L_s \tag{6}$$

$$\frac{\partial c_1}{\partial x} = \varepsilon^{3/2} \frac{\partial c_2}{\partial x} \quad \text{at } x = L_s \tag{7}$$

Dimensionless parameters are defined as follows:

$$\Theta = \frac{c}{c_0}, \quad y = \frac{x}{L_s}, \quad r = \frac{L_+}{L_s}$$
$$\tau = \frac{Dt}{L_s^2}, \quad J = \frac{a(1 - t_+^0) L_s^2 j_n}{\varepsilon D c_0} \tag{8}$$

Then the differential equation and boundary conditions become

$$\frac{\partial \Theta_2}{\partial \tau} = \varepsilon^{1/2} \frac{\partial^2 \Theta_2}{\partial y^2} + J \tag{9}$$

in the porous electrode and

$$\frac{\partial \Theta_1}{\partial \tau} = \frac{\partial^2 \Theta_1}{\partial y^2} \tag{10}$$

in the separator. The boundary conditions become

$$\frac{\partial \Theta_2}{\partial y} = 0 \quad \text{at } y = 1 + r \tag{11}$$

$$\frac{\partial \Theta_1}{\partial y} = -\gamma \text{ with } \gamma = \frac{I(1 - t_+^0) L_s}{F D c_0} \quad \text{at } y = 0 \tag{12}$$

$$\Theta_1 = \Theta_2 = 1 \quad \text{at } \tau = 0 \tag{13}$$

$$\Theta_1 = \Theta_2 \quad \text{at } y = 1 \tag{14}$$

$$\frac{\partial \Theta_1}{\partial y} = \varepsilon^{3/2} \frac{\partial \Theta_2}{\partial y} \quad \text{at } y = 1 \tag{15}$$

The function J needs to be specified to evaluate the solution to Equations 9 and 10.

The reaction rate distribution in the porous electrode can be complex as it reflects the tradeoff between ohmic and kinetic resistances as well as solution-phase concentration variations. However, a uniform current distribution results when using an insertion material having an open circuit potential that depends strongly on the state of charge of the system [6]. Newman [18] has shown that a uniform current distribution can be expected when kinetic resistances dominate ohmic resistances. In either case it is possible to assume that j_n is given by its average value everywhere in the porous electrode

$$j_n = \frac{-I}{aFL_+} \text{ or } J = \frac{-\gamma}{\varepsilon r} \tag{16}$$

We make this assumption here and later consider the opposite case of the extreme nonuniform current distribution (the Stein analysis) for comparison.

Solving Equations 9 and 10 to find the steady state solution $(\partial/\partial t = 0)$ we obtain

$$\Theta_1 = B - \gamma y \tag{17}$$

and

$$\Theta_2 = E - \frac{J}{\varepsilon^{1/2}} \left[\frac{y^2}{2} - (1+r)y \right] \tag{18}$$

where the constants are

$$B = 1 + \gamma \left[1 - \frac{1}{2(1+\varepsilon r)} - \frac{r^2}{3\varepsilon^{1/2}(1+\varepsilon r)} \right] \tag{19}$$

$$E = 1 - \frac{J\varepsilon r}{2(1+\varepsilon r)} + \frac{J}{\varepsilon^{1/2}(1+\varepsilon r)} \times \left[\frac{\varepsilon}{3} + \frac{\varepsilon r}{2} - r - \frac{1}{2} - \frac{\varepsilon(1+r)^3}{3} \right] \tag{20}$$

Subscript 1 denotes the separator region and 2 refers to the porous electrode region. Example steady state concentration profiles are given in Fig. 2 for the model system described in Appendix A. The concentration profiles scale with the current and pivot around a point that depends on the values of r and ε, which in this example are $r = 4$ and $\varepsilon = 0.5$.

The concentration has a minimum value at the back of the porous electrode $(y = 1 + r)$. This value can be used to check whether the concentration is driven to zero during the discharge, as for the highest current shown in Fig. 2. If this concentration at the back is greater than zero, then the cell is not limited by solution-phase transport and discharges until either all the capacity is consumed or the cutoff potential is exceeded. If it useful to express this in terms of a 'limiting' current, below which the concentration is not driven to zero at steady state,

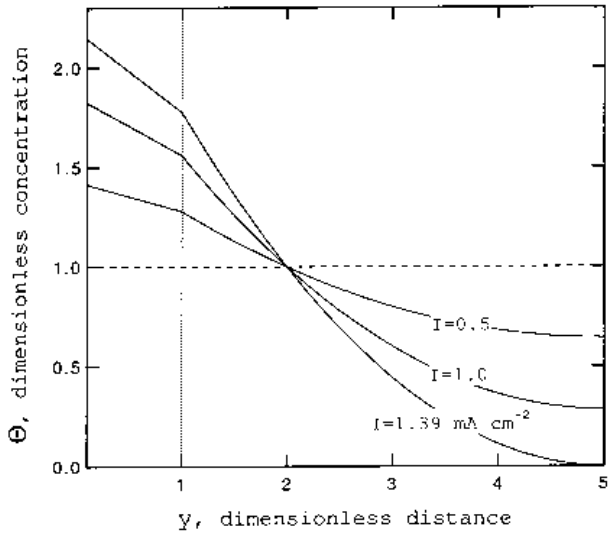

Fig. 2. Steady state concentration profiles across the full cell for galvanostatic discharges at various current densities. Separator/positive electrode boundary: dotted line. System parameters: see Appendix A.

$$I = \frac{FDc_0}{(1 - t_+^0) L_s f(r, \varepsilon)} \tag{21}$$

where

$$f(r,\varepsilon) = \frac{1}{2(1+\varepsilon r)} + \frac{(1+r)^2}{2r\varepsilon^{3/2}} + \frac{1}{r\varepsilon^{3/2}(1+\varepsilon r)} \left[\frac{\varepsilon}{3} + \frac{\varepsilon r}{2} - r - \frac{1}{2} - \frac{\varepsilon(1+r)^3}{3} \right] \tag{22}$$

Note the analogy between the limiting current at a flat electrode and that in a porous electrode given in Equation 21. The latter value is reduced by the factor f, which is a function of the geometric parameters of the porous electrode only and approaches 0.5 as $r \to 0$. This limit as $r \to 0$ is the correct result for the limiting current to a planar electrode. Figure 3

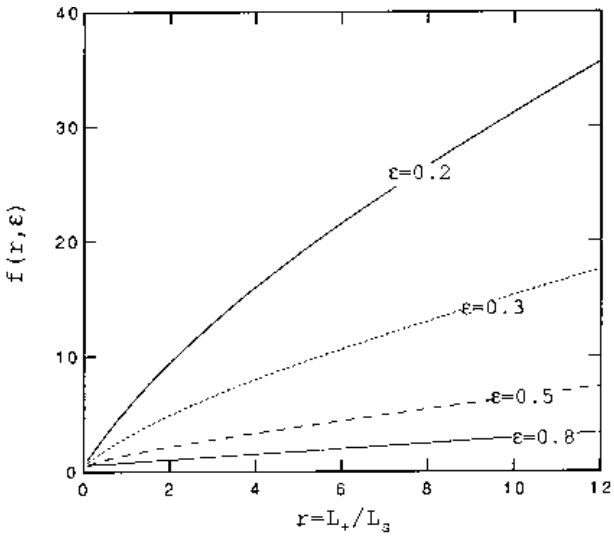

Fig. 3. Limiting current in the porous electrode is reduced by factor f, given above as a function of the geometric parameters ε and r (ratio of positive electrode to separator thickness).

demonstrates the behaviour of the function $f(r, \varepsilon)$ as a function of r for various values of ε.

The full problem can be solved by expressing the problem in terms of the new variable

$$A(\tau, y) = \Theta(\tau, y) - \Theta_{ss}(y) \tag{23}$$

Θ_{ss} is defined as the steady state solution given in Equations 17 and 18. The equation then becomes

$$\frac{\partial A_2}{\partial \tau} = \varepsilon^{1/2} \frac{\partial^2 A_2}{\partial y^2} \tag{24}$$

in the porous electrode and

$$\frac{\partial A_1}{\partial \tau} = \frac{\partial^2 A_1}{\partial y^2} \tag{25}$$

in the separator. The boundary conditions are

$$\frac{\partial A_1}{\partial y} = 0 \quad \text{at } y = 0 \tag{26}$$

$$\frac{\partial A_2}{\partial y} = 0 \quad \text{at } y = 1 + r \tag{27}$$

$$A_1 = A_2 = 1 - \Theta_{ss}(y) \quad \text{at } \tau = 0 \tag{28}$$

$$A_1 = A_2 \quad \text{at } y = 1 \tag{29}$$

$$\frac{\partial A_1}{\partial y} = \varepsilon^{3/2} \frac{\partial A_2}{\partial y} \quad \text{at } y = 1 \tag{30}$$

The transient problem is solved by separation of variables: the solution has the form

$$A_1(\tau, y) = \sum_{n=1}^{\infty} F_n \exp(-\lambda_n^2 \tau) \cos(\lambda_n y) \tag{31}$$

$$A_2(\tau, y) = \sum_{n=1}^{\infty} G_n \exp(-\lambda_n^2 \tau) \cos[\lambda_n (1 + r - y)] \tag{32}$$

The constants F_n and G_n are determined by using the orthogonality condition of the eigenfunctions:

$$F_n = \frac{2[(1 - B)\lambda_n \sin(\lambda_n) + \gamma \cos(\lambda_n) + \gamma \lambda_n \sin(\lambda_n) - \gamma]}{\left[\lambda_n^2 + \frac{1}{2}\lambda_n \sin(2\lambda_n)\right]} \tag{33}$$

$$\begin{aligned} G_n =& (1 - E)\sin(\lambda_n r) + \frac{J}{2\varepsilon^{1/2}\lambda_n^2}[2y\lambda_n \cos(\lambda_n(1 + r - y)) \\ &+ 2\sin(\lambda_n(1 + r - y)) - \lambda_n^2 y^2 \sin(\lambda_n(1 + r - y))] \\ &+ \frac{J(1 + r)}{\varepsilon^{1/2}}\left[\frac{(\cos(\lambda_n r) - 1)}{\lambda_n} - \sin(\lambda_n r)\right] \end{aligned} \tag{34}$$

The matching conditions at $y = 1$ provide a generating equation for the eigenvalues

$$\tan(\lambda_n) = -\varepsilon^{5/4} \tan(\varepsilon^{-1/4} \lambda_n r) \tag{35}$$

The first few eigenvalues are sufficient for our purposes; for $r = 4$ and $\varepsilon = 0.5$ these are

$$\begin{aligned} &\lambda_1 = 0.32566, \quad \lambda_2 = 0.80905, \\ &\lambda_3 = 1.31882, \quad \lambda_4 = 1.83231 \end{aligned} \tag{36}$$

The time for the concentration at the back face to reach zero is the relevant quantity for our analysis. This situation occurs only if the discharge rate is above the 'limiting' current (see Equation 21). For rates near the limiting current it is sufficient to use only a single eigenvalue when calculating the time to deplete the solution. Then, the time is given by

$$\tau_d = \frac{1}{\lambda_1^2} \ln\left[\frac{-G_1}{\Theta_{2,ss}(y = 1 + r)}\right] \tag{37}$$

When operating much higher than the limiting current it becomes increasingly difficult to use Equation 32 to determine the discharge time because of the need to evaluate an increasing number of terms in the equation. In this case it is easier to examine a short-time solution to the original differential equations. Using a Laplace transformation and then taking the inverse transform for large values of s, the solution-phase concentration at the back of the positive electrode is

$$\Theta_2 = 1 + J\tau \quad \text{at } y = 1 + r \tag{38}$$

This gives a depletion time of

$$\tau_d = \frac{-1}{J} \tag{39}$$

These two expressions are used to construct Fig. 4, which gives the time to deplete the solution as a function of the ratio of the limiting current to the cell current. The limiting current for the present example system (see Appendix A) is calculated from Equation 21 to be $I_{lim} = 1.12\,\text{mA cm}^{-2}$. Although the full Equation 32 may be used to generate this figure more accurately over the whole range, these two approximate expressions are capable of capturing the full behaviour of the system. This approximation also avoids the use of numerical computations to evaluate the series developed above.

For systems limited by solution-phase transport we can equate the time t_d with the discharge time and use this in an expression for the system's capacity. The specific capacity is the product of the current

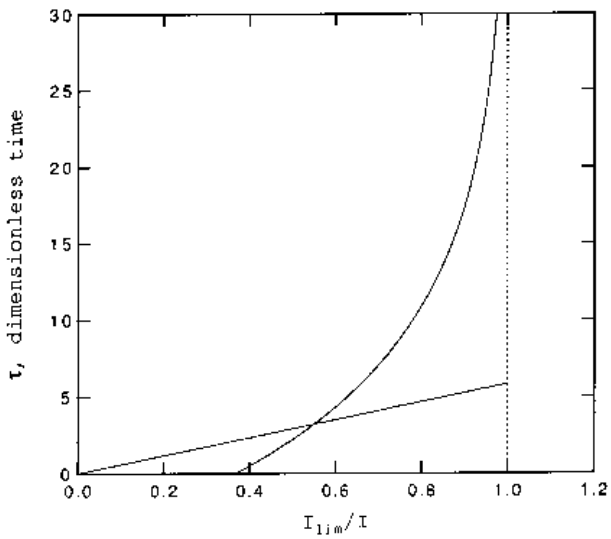

Fig. 4. Time to reach zero concentration at the back of the positive electrode is plotted from Equation 37, which uses only a single eigenvalue, and the short time solution given by Equation 39, as a function of the discharge rate. $I_{lim} = 1.12\,\text{mA cm}^{-2}$ for $r = 4$ and $\varepsilon = 0.5$.

density and the discharge time divided by the mass per unit area

$$C = \frac{It_d}{M} \tag{40}$$

For this work we take the mass to include the separator and positive electrode only,

$$M = \rho_s L_s + \left[\varepsilon\rho_s + (1-\varepsilon)\rho_+\right]L_+ \tag{41}$$

giving $M = 0.059\,\mathrm{g\,cm^{-2}}$ for the present example system. Figure 5 is the resulting capacity–rate behaviour of the system. There are three distinct regions of the plot. At low rates (when $I < I_{lim}$), the capacity is completely exhausted during the discharge, and thus the maximum capacity is attained. The maximum capacity for this system is calculated to be $C_{max} = 299.6\,\mathrm{C\,g^{-1}}$. As the limiting current is exceeded, the capacity drops off steeply with increasing rate. A break in the curve occurs when the single eigenvalue solution is replaced by the short-time solution. Because the short-time solution found the depletion time to be inversely proportional to the current density, the capacity appears to be independent of rate at these very high rates. This unusual result does not happen in real systems because of the increasing ohmic drop, which eventually dominates the discharge time.

These short-time results for a uniform reaction rate distribution are compared with the Stein short-time case [14]. Stein originally examined the possibility of failure of the lead-acid battery due to the depletion of the acid in the pores at the front of the positive electrode. In our adaptation of the Stein case the reaction-rate distribution is described by a delta function at the separator/positive electrode boundary. This reaction distribution represents the extreme case of a solution-phase ohmically-limited system and is thus more likely to approximate the actual reaction distribution at very high rates than the uniform case. In contrast to the previous case (see Appendix B), for this case the depletion time depends on the inverse of current squared,

$$t_d = \frac{\pi F^2 D c_0^2}{4(1-t_+^0)^2 I^2}\left[1+\varepsilon^{5/4}\right]^2 \tag{42}$$

This implies a capacity that is inversely proportional to the discharge rate at high rates, or a slope of −1 on the log-log capacity–rate plot (see Fig. 5).

A variation of this behaviour is to have a sharp reaction zone moving through the positive electrode as the capacity is consumed locally. This is a more physically realistic extension of the Stein analysis because local concentration variations, both in solution and in the solid phase (if applicable), cause the reaction to shift to other regions of the porous electrode. A quasisteady state analysis of the moving-zone case provides an analytic solution for the capacity-rate behaviour (details in Appendix C). A new parameter q, the capacity density of the composite electrode, arises in this case.

The Stein case and the uniform-reaction-rate distribution case are two limits of a continuum of behaviour, each valid over only a small range of parameter space. Because the reaction zone cases correspond more closely to a high rate discharge we more likely expect to see this high rate asymptotic behaviour for solution-phase diffusion limitations on a capacity–rate plot. For a concentrated reaction zone the Stein result should be a lower limit on capacity. If the time of discharge is long enough, so that the product Dt_d approaches or exceeds L_s^2, the region of concentration depletion will extend to the anode, where there is an unlimited supply of lithium ions. Consequently, for a sharp reaction zone the results should follow the maximum capacity at the upper left of Fig. 5, then follow (at higher rates) the moving zone results and, finally, follow the Stein results (at the bottom right). There never would be a rate (for electrolyte depletion) beyond which the cell would fail instantaneously (zero capacity). As parameters are shifted from those on which Fig. 5 was based, the region of the moving zone model may shrink or expand, particularly as q is changed, q being a parameter absent from all the curves on Fig. 5 except the moving zone curve (and the maximum capacity line).

Figure 5 also shows that the uniform reaction distribution permits the largest discharge rate before concentrations manifest themselves. This is appropriate since any focusing of the reaction rate compromises the ability of the system to deplete the electrolyte at the back of the positive electrode.

The above result for the specific capacity can be used to express the specific energy of the system as a function of discharge rate. This requires an estimate of the average cell potential during discharge. The cell potential may simply be taken as the average of the open circuit value and the cutoff potential; then the specific energy is directly proportional to the capacity.

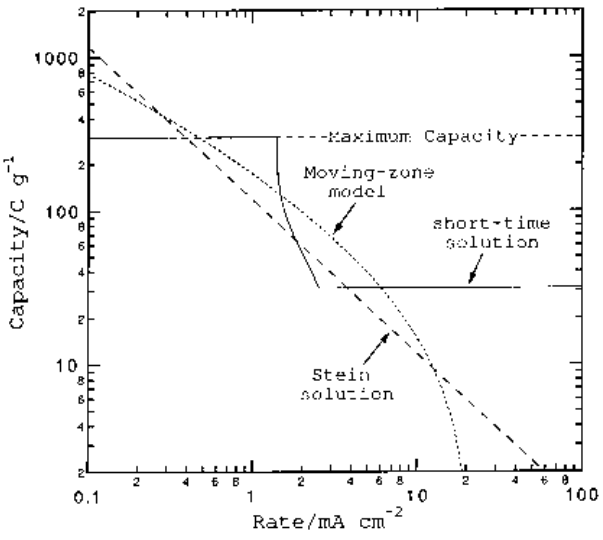

Fig. 5. Model predictions for capacity against discharge rate of a cell limited by solution-phase diffusion. Reaction distribution in positive electrode is assumed to be uniform for the solid line. Dashed lines: Stein[14] result and moving zone result. $M = 0.059\,\mathrm{g\,cm^{-2}}$.

Alternatively, more sophisticated approaches may be taken, accounting for the effect of the discharge rate on the average cell potential through ohmic drop and concentration overpotential. The larger of these overpotentials is the dominant loss of energy in the cell. A more sophisticated approach like this requires further assumptions about the system (and hence more parameters). We also quickly lose the simplicity that was the advantage of these limiting cases. For these reasons, we will not attempt to estimate the specific energy, but leave the results here and those to follow in terms of the specific capacity.

3.2. *Case II: Solid-phase diffusion limitations*

It is possible for the discharge of a cell to be limited by diffusion of lithium into the insertion electrode structure. This was a major limitation to the high rate discharge of early cells using nonporous thin film electrodes. Among the advantages of the porous electrode configuration is the small particle size and reduced diffusion length in the electrode phase. This reduces the solid-phase diffusion limitations somewhat; a measure of their importance can be found from the parameter [6, 7]

$$S_s = \frac{R_s^2 I}{D_s F(1-\varepsilon)c_t L_+} \tag{43}$$

a ratio of the time of discharge to the time constant for diffusion. For $S_s \ll 1$, diffusion in the solid phase is sufficiently fast, and it is possible to neglect the impact of solid-phase diffusion limitations on the discharge.

If severe diffusion limitations exist the battery capacity may be estimated by relating the discharge time to the time to reach a limiting current in the solid phase. The reaction rate distribution in the porous electrode is assumed uniform and equal to its average value (Equation 16). We also assume the diffusion coefficient of lithium in the insertion material is a constant. The mathematical formulation of the problem is then

$$\frac{\partial c_s}{\partial t} = \frac{D_s}{r^2}\frac{\partial}{\partial r}\left[r^2\frac{\partial c_s}{\partial r}\right] \tag{44}$$

Boundary conditions include

$$\frac{\partial c_s}{\partial r} = 0 \text{ at } r = 0 \tag{45}$$

$$D_s\frac{\partial c_s}{\partial r} = \frac{I}{aFL_+} \text{ at } r = R_s$$

$$c_s = c_s^0 \text{ at } t = 0$$

A solution to this problem can be found [20], but it is expressed as an infinite series that is cumbersome to evaluate.

As in case I we develop solutions to Equation 44 that are valid for short and long times; these illustrate the behaviour of the system without being too complicated to be useful. For short discharge times, or high rates, a planar diffusion model is valid, giving the following relationship between discharge time and rate

$$t_d = \frac{\pi c_t^2 F^2 D_s a L_+}{4I^2} \tag{46}$$

The surface area per unit volume for the porous electrode is related to the particle size through

$$a = \frac{n(1-\varepsilon)}{R_s} \tag{47}$$

where $n = 1, 2$ or 3 for planar, cylindrical or spherical particles, respectively. For cylindrical and planar particles, R_s is half the shortest characteristic length of the particle. Disc-shaped particles, whose thickness is less than their radius, should be treated as planar. From this we find

$$C = \frac{It_d}{M} = \frac{\pi c_t^2 F^2 D_s n(1-\varepsilon)L_+}{4MR_s I} \tag{48}$$

where the mass M is given by Equation 41, for example. Thus, the capacity is inversely proportional to the rate at high rates.

For longer times, or lower rates, a pseudo-steady-state is established in the particles. This leads to a steady concentration profile of the form

$$c_s(r=0) - c_s(r) = \frac{-Ir^2}{2aFD_sL_+R_s} \tag{49}$$

The discharge time is approximated as the time for the concentration of lithium at the surface to reach the maximum value. The capacity is then calculated from

$$C = \frac{F\varepsilon_+ L_+}{M}\left[\bar{c}_s - c_s^0\right] \tag{50}$$

with $\bar{c}_s$ representing the average concentration of lithium in the solid at the end of discharge. This leads to

$$C = \frac{F\varepsilon_+ L_+}{M}\left[c_t - c_s^0 - \frac{3R_s I}{10aFD_sL_+}\right] \tag{51}$$

In Fig. 6, the two solutions developed above are plotted as the logarithm of the specific capacity against the logarithm of the discharge rate. The parameters used to generate Fig. 6 are given in Appendix A; the cell is again the Li|$LiMn_2O_4$ system. Figure 6 has the expected behaviour at low rates, where the capacity approaches the theoretical maximum value. At higher rates the capacity–rate plot has a slope of −1. The high rate asymptotes for both this solid state diffusion problem and the Stein solution-phase diffusion model (Appendix B) have identical slopes of −1. However, the low rate regions of the capacity–rate plot have different forms. In general, a higher capacity is attained in case II than in case I at a given rate with the present set of parameter values (cf. Figs 5 and 6). This indicates that solid state diffusion limitations are not as restrictive as solution-phase diffusion limitations in this system.

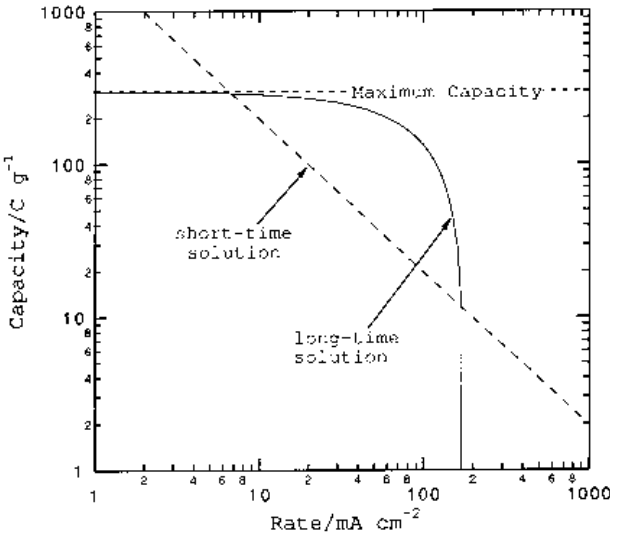

Fig. 6. Log-log capacity–rate plot for a hypothetical system limited by solid state diffusion in electrode particles. The two lines come from analytic solutions for short and long times, respectively. $M = 0.059\,\mathrm{g\,cm^{-2}}$.

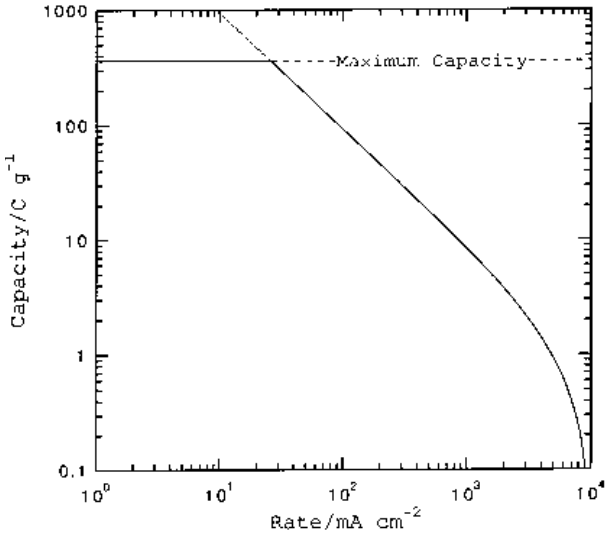

Fig. 7. Theoretical capacity–rate plot for lithium/polymer/lithium–manganese oxide system with no concentration gradients. Dotted line: prediction of reaction zone model; dashed line: maximum specific capacity. Solid line results from combining the reaction zone model with a maximum capacity condition. $M = 0.031\,\mathrm{g\,cm^{-2}}$.

3.3. *Case III: Ohmically-dominated reaction zone model*

The neglect of concentration gradients represents a great simplification in the theoretical treatment. This assumption will hold for any system with a unity transference number for the lithium ion; several polymer electrolytes have been developed that fulfill this condition [21]. With this assumption, as well as those given previously, the system is ohmically dominated. The insertion reaction moves through the porous electrode like a spike, consuming all the active material before moving on. This continues until either the cutoff potential is reached or the active material is completely consumed [10, 11].

Analysis details have been published previously [15]; for this work we simply use the final results. The cell potential for an ohmically-dominated system with a linear open circuit potential is

$$V = U^{\theta} - \frac{IL_s}{\kappa_s} - \frac{I^2 t}{\kappa q} \tag{52}$$

The cell potential is independent of the slope of the open circuit potential curve, and hence becomes identical to that used in [11].

Setting the cell potential in Equation 52 equal to the cutoff potential determines the time of discharge,

$$t_d = \frac{\kappa q}{I^2}\left[U^{\theta} - V_c - \frac{IL_s}{\kappa_s}\right] \tag{53}$$

As with the previous cases an expression for the discharge time of the battery provides a means for calculating the capacity

$$C = \frac{It_d}{M} = \frac{\kappa q}{IM}\left[U^{\theta} - V_c - \frac{IL_s}{\kappa_s}\right] \tag{54}$$

Equation 54 is the basis for the capacity-rate plot given as Fig. 7. The system under consideration, described in Appendix A, is a lithium/manganese oxide cell with a solid polymer electrolyte. The dashed line on Fig. 7 indicates the maximum specific capacity ($360.1\,\mathrm{C\,g^{-1}}$) that the system can provide, calculated by assuming a useful manganese oxide stoichiometry of $0.2 \le y \le 1.0$ in $Li_yMn_2O_4$. A substantial portion of the capacity–rate plot has a slope of -1. At very high current densities, the maximum discharge rate is approached, and the curve bends over and becomes vertical.

The specific capacity given by Equation 54 continues to increase at lower discharge rates because it neglects the finite amount of active material in the cell, corresponding to the dotted line on Fig. 7. Thus, the specific capacity must bend over at lower rates and approach the maximum specific capacity indicated on the figure, as shown by the solid curve. The discharge time chosen to be the lower of Equation 54 and

$$t_d = \frac{qL_+}{I} \tag{55}$$

gives the expected behaviour of the capacity–rate plot.

4. Comparison among cases

The utility of limiting cases developed above is in the analysis and correlation of experimental capacity–rate data. First, experimental data may possibly be used to distinguish among the phenomena dominating the discharge of a battery. Second, simplified expressions of this form have been used in the design and optimization process, as a means of assessing the impact on the performance of varying system parameters [6, 10, 11]. However, a more detailed mathematical model is generally required for the final optimization of the battery design. This arises natu-

rally as the optimum design will usually be one in which several phenomena are balanced against one another, and no single phenomenon (i.e., ohmic drop, diffusion in the solution phase, etc.) dominates the battery behaviour.

There are many similarities in the results for the above cases. In each case, the capacity reaches its maximum value at low rates and decreases towards zero at high rates. Regions of the log-log capacity–rate plot where the slope is -1 are seen in each case. The ohmically-dominated case has a region of slope -1 whose size varies based on the parameters employed; in general this region becomes larger for thicker and less porous electrodes. These features make it difficult to distinguish among the various phenomena based on qualitative features of the capacity–rate data.

Dimensionless parameters can be developed and used to determine the dominant limitation in the battery. We can, for example, use the high-rate asymptotes found earlier to determine which phenomenon is limiting for a given system based on the values of certain parameters. One way to proceed is to make a direct comparison between log-log capacity–rate plots for each case. The discharge time varies with the current density in a similar manner at high rates for each case, which can be seen by comparing Equations 42, 46 and 54. We assume that, for a given system, the smallest of these discharge times is dominant. We use the result from the Stein analysis to represent the aysmptotic behaviour of a system dominated by solution-phase diffusion limitations. Then, the relative magnitudes of the constants preceding the above expressions for discharge time against I^{-2} determine the dominant phenomenon.

A log-log plot of the ratios of these constants separates the overall behaviour of the system into three categories: ohmically dominated, solid-phase diffusion dominated and solution-phase diffusion dominated. Figure 8 shows the three regions of behaviour. Interfacial kinetic resistances have been neglected. The two ratios plotted are

$$r_1 = \frac{\varepsilon^{7/2}}{3\varepsilon_+}\left[\frac{c_0}{c_t}\right]^2 \frac{1}{(1-t_+^0)^2}\frac{DR_s}{D_s L_+} \tag{56}$$

a ratio of solid to solution-phase diffusion times, and

$$r_2 = \frac{\pi\varepsilon^{7/2}F^2 D c_0}{4(1-t_+^0)^2 \kappa q U^\theta (1 - V_c/U^\theta)} \tag{57}$$

a ratio of ohmic drop to solution-phase diffusion. We neglect the ohmic drop through the separator in Equation 54 to allow the dimensionless ratios to be independent of discharge rate. The region in which a system operates is determined from these dimensionless parameters. The limiting cases considered above provide only approximate expressions, and for systems that are near, or on the border, between two or more phenomena, this simplified treatment will not hold.

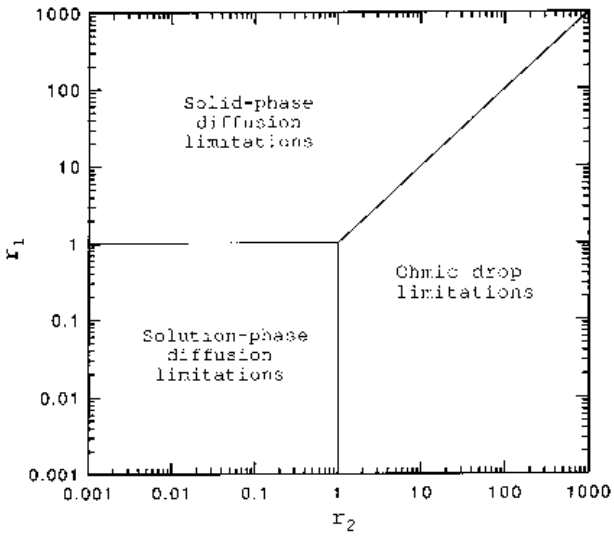

Fig. 8. Log-log plot describing the regions of dominant phenomena in terms of two dimensionless time constant ratios. Ordinate: tradeoff between solution and solid-phase diffusion; abscissa describes ratio of solution-phase diffusion limitations to ohmic drop.

Acknowledgement

This work was supported by the Assistant Secretary for Energy Efficiency and Renewable Energy, Office of Transportation Technologies, Office of Advanced Automotive Technologies of the U.S. Department of Energy under Contract No. DE-AC03-76SF00098.

References

[1] R. Selim and P. Bro, *J. Electrochem. Soc.* **118** (1971) 829.
[2] D. Linden (ed.),'Handbook of Batteries', 2nd edn, McGraw-Hill, New York (1995).
[3] G. W. Vinal, 'Storage Batteries', 4th edn, J. Wiley & Sons, New York (1995), p.216.
[4] M. Z. A. Munshi and B. B. Owens, *Solid State Ion.* **38** (1990) 103.
[5] M. Doyle, T. F. Fuller and J. Newman, *J. Electrochem. Soc.* **140** (1993) 1526.
[6] T. F. Fuller, M. Doyle and J. Newman, *ibid.* **141** (1994) 1.
[7] *Idem*, *ibid.* **141** (1994) 982.
[8] M. Doyle, T. F. Fuller and J. Newman, *Electrochim. Acta* **39** (1994) 2073.
[9] M. Doyle, J. Newman, A. S. Gozdz, C. N. Schmutz and J.-M. Tarascon, *J. Electrochem. Soc.* **143** (1996) 1890.
[10] W. Tiedemann and J. Newman, *ibid.* **122** (1975) 1482.
[11] J. Newman, *ibid.* **142** (1995) 97.
[12] J. Newman and C. W. Tobias, *ibid.* **109** (1962) 1183.
[13] R. Pollard and J. Newman, *Electrochim. Acta* **25** (1980) 315.
[14] W. Stein, *Naturwissenschaften* **45** (1958) 459.
[15] M. Doyle and J. Newman, *J. Power Sources* **54** (1995) 46.
[16] S. Atlung, B. Zachau-Christiansen, K. West and T. Jacobsen, *J. Electrochem. Soc.* **131** (1984) 1200.
[17] B. C. Knutz, K. West, B. Zachau-Christiansen and S. Atlung, *J. Power Sources* **43–44** (1993) 733.
[18] J. Newman, '*Electrochemical Systems*', Prentice Hall, Englewood Cliffs, N. J. (1991).
[19] D. A. G. Bruggeman, *Ann. Phys.* **24** (1935) 636.
[20] H. S. Carslaw and J. C. Jaeger, 'Conduction of Heat in Solids', Clarendon Press, Oxford (1959), p. 242.
[21] F. M. Gray, '*Solid Polymer Electrolytes*', VCH, New York (1991).
[22] A. Bouridah, F. Dalard, D. Deroo and M. B. Armand, *J. Appl. Electrochem.* **17** (1987) 625.
[23] D. Guyomard and J. M. Tarascon, *J. Electrochem. Soc.* **139** (1992) 937.

Appendix A: Parameters used in the models

We modelled a system with a lithium foil negative electrode, a solid polymer electrolyte separator and a lithium-manganese-oxide composite positive electrode. In the simplified treatment of case I, the transport properties are assumed to be constant and equal to their values at the initial concentration. Thus, the salt diffusion coefficient is 7.5×10^{-8} $\mathrm{cm^2\,s^{-1}}$ [22], and the transference number is 0.2 [22]. The system parameters used in this case include $L_s = 50\ \mu\mathrm{m}$, $L_+ = 200\ \mu\mathrm{m}$, $\varepsilon = 0.5$, and $c_0 = 2\ \mathrm{mol\,dm^{-3}}$. Densities for the positive electrode and separator used to calculate the system's mass are $\rho_+ = 4.1\ \mathrm{g\,cm^{-3}}$ and $\rho_s = 1.2\ \mathrm{g\,cm^{-3}}$. The useful range of positive electrode stoichiometry is assumed to equal $0.20 \le y \le 1.0$ in $Li_yMn_2O_4$. This gives a maximum specific capacity of $1767.6\ \mathrm{C\,cm^{-3}}$ for the positive electrode material, or $299.6\ \mathrm{C\,g^{-1}}$ based on the mass of the composite positive electrode (polymer plus active material). Conducting additives and binders are not included in the present treatment.

For case II, the solid-state diffusion coefficient of lithium in the lithium–manganese oxide spinel is $1 \times 10^{-9}\ \mathrm{cm^2\,s^{-1}}$ [23]. In addition to the values given for case I, other parameters needed are an average particle radius, $R_s = 10\ \mu\mathrm{m}$, the theoretical maximum solid concentration, $c_t = 22.9\ \mathrm{mol\,dm^{-3}}$, and the surface area per unit volume for the porous electrode, $a = 1.5 \times 10^3\ \mathrm{cm^{-1}}$.

The separator for case III is an idealized polymer with a unity lithium ion transference number, a conductivity of $4.0 \times 10^{-5}\ \mathrm{S\ cm^{-1}}$, and a separator thickness of $10\mu\mathrm{m}$. The capacity density of the lithium-manganese-oxide electrode is taken to be $q = 1767.6\ \mathrm{C\ cm^{-3}}$; this equates to $360.1\ \mathrm{C\ g^{-1}}$ based on the composite positive electrode mass. The initial open circuit potential is 4.0 V and the cutoff potential used is 2.0 V. The values of the electrode thickness ($L_+ = 95.4\ \mu\mathrm{m}$) and porosity ($\varepsilon = 0.338$) are obtained by maximizing the cell's specific energy for a 3 h dicharge time. The mass per unit area of the cell, calculated using Equation 41 in the text, is $0.031\ \mathrm{g\,cm^{-2}}$.

Appendix B: Derivation of the Stein analysis

Under very high rate discharges, a battery may shut off due to depletion of the active species at the front face of the porous electrode. This situation was first considered by Stein [14], where it was applied to the lead–acid battery. One interpretation of the Stein case is presented here. We assume the reaction is confined to a thin region at the electrode/separator boundary. Thus,

$$j_n = \frac{-I\delta(x - L_s)}{aF} \tag{B-1}$$

where $\delta(x)$ represents the Dirac delta function.

The Laplace transform of Equation 9 with $J = 0$ is

$$s\bar{\Theta}_2(s,y) - 1 = \varepsilon^{1/2}\frac{\partial^2\bar{\Theta}_2}{\partial y^2} \tag{B-2}$$

This has the solution

$$\bar{\Theta}_2 = \frac{1}{s} + A_2(s)\left[\exp - \frac{(y-1)s^{1/2}}{\varepsilon^{1/4}}\right] \tag{B-3}$$

The Laplace transform of Equation 10 is

$$s\bar{\Theta}_1(s,y) - 1 = \frac{\partial^2\bar{\Theta}_1}{\partial y^2} \tag{B-4}$$

with the solution

$$\bar{\Theta}_1 = \frac{1}{s} + A_1(s)\left[\exp(y-1)s^{1/2}\right] \tag{B-5}$$

Application of continuity of concentration at $y = 1$ gives

$$A_1(s) = A_2(s) = A(s) \tag{B-6}$$

The value of the constant is found by applying continuity of flux at the boundary $y = 1$. The balance on the flux of cations (or anions) is related to the current density through

$$\frac{I}{F} = N_+(y = 1_-) - N_+(y = 1_+) \tag{B-7}$$

which becomes

$$\frac{I}{F} = -D\frac{\partial c}{\partial x}(y = 1_-) + \frac{t_+^0 I}{F} - \left[-\varepsilon^{3/2}D\frac{\partial c}{\partial x}(y = 1_+)\right] \tag{B-8}$$

Expressed in terms of the dimensionless variables from the text,

$$\frac{\gamma}{s} = -\frac{\partial\bar{\Theta}_1}{\partial y}(y = 1_-) + \varepsilon^{3/2}\frac{\partial\bar{\Theta}_2}{\partial y}(y = 1_+) \tag{B-9}$$

Substitution of the partial derivatives of Equations B-3 and B-5 leads to

$$\frac{\gamma}{s} = -A(s)s^{1/2}\left[1 + \varepsilon^{5/4}\right] \tag{B-10}$$

and also

$$\bar{\Theta}_2(y = 1, s) = \frac{1}{s} - \frac{\gamma}{s^{3/2}}\frac{1}{1 + \varepsilon^{5/4}} \tag{B-11}$$

The inverse Laplace transform of Equation B-11 is

$$\Theta_2(y = 1, \tau) = 1 - 2\gamma\left[\frac{\tau}{\pi}\right]^{1/2}\frac{1}{1 + \varepsilon^{5/4}} \tag{B-12}$$

leading to the transition time

$$\tau_d = \frac{\pi}{4\gamma^2}\left[1 + \varepsilon^{5/4}\right]^2 \tag{B-13}$$

This is written in dimensional terms in Equation 42.

Appendix C: Derivation of the moving-zone model

In the moving-zone analysis, a sharp reaction zone moves through the positive electrode consuming all the available capacity before moving on. The concentration distribution ahead of the zone is uniform, while that behind the zone obeys the conservation of

mass condition for a quasisteady state profile. This gives a linear concentration in each region, related to the current density by

$$\frac{I}{F} = -\frac{\varepsilon^{3/2} D}{1 - t_+^0} \frac{\mathrm{d}c}{\mathrm{d}x} = -\frac{D}{1 - t_+^0} \frac{\mathrm{d}c}{\mathrm{d}x} \qquad \text{(C-1)}$$

where the middle expression corresponds to the positive electrode and the right expression to the separator. Using this result, the concentration profile is

$$c = c_1 \quad \text{for } L_s + x_r < x < L_s + L_+ \qquad \text{(C-2)}$$

$$c = c_1 + \frac{I(1 - t_+^0)}{FD\varepsilon^{3/2}} (x_r - x + L_s) \quad \text{for } L_s < x < L_s + x_r$$

$$c = c_1 + \frac{I(1 - t_+^0)}{FD} \left[\frac{x_r}{\varepsilon^{3/2}} - x + L_s \right] \quad \text{for } 0 < x < L_s$$

The position of the reaction zone, x_r, is measured with respect to the positive electrode–separator interface.

Application of conservation of mass provides an additional restriction on the concentration profile and relates c_1 to c_0. By setting $c_1 = 0$ in the above expression, the position of the reaction zone x_r at the end of discharge as a function of the current density I is obtained. To be meaningful, the reaction zone position must be less than L_+.

The position of the zone is given by

$$x_r = -\frac{L_s}{\varepsilon} + \left[\frac{L_s^2}{\varepsilon^2} - L_s^2 \varepsilon^{1/2} + \frac{2c_0(\varepsilon L_+ + L_s) FD\varepsilon^{1/2}}{I(1 - t_+^0)} \right]^{1/2} \qquad \text{(C-3)}$$

The capacity consumed by the reaction may be expressed in terms of the reaction zone position as

$$C = \frac{x_r}{L_+} \frac{qL_+\varepsilon_+}{M} \qquad \text{(C-4)}$$

This capacity is plotted in Fig. 5 in the text.